Microstructured waveguides in *z*-cut $LiNbO_3$ by high-repetition rate direct femtosecond laser inscription

Mykhaylo Dubov,* Sonia Boscolo, and David J. Webb

Aston Institute of Photonic Technologies, School of Engineering and Applied Science, Aston University, Birmingham B4 7ET, UK

*m.dubov@aston.ac.uk

Abstract: We report on the operational parameters that are required to fabricate buried, microstructured waveguides in a z-cut lithium niobate crystal by the method of direct femtosecond laser inscription using a high-repetition-rate, chirped-pulse oscillator system. Refractive index contrasts as high as -0.0127 have been achieved for individual modification tracks. The results pave the way for developing microstructured WGs with low-loss operation across a wide spectral range, extending into the mid-infrared region up to the end of the transparency range of the host material.

OCIS codes: (220.4000) Microstructure fabrication; (230.7370) Waveguides; (130.5296) Photonic crystal waveguides; (190.4390) Nonlinear optics, integrated optics.

References and links

1. R. Osellame, G. Cerullo, and R. Ramponi, eds., *Femtosecond Laser Micromachining: Photonic and Microfluidic Devices in Transparent Materials* (Springer-Verlag, 2012).
2. H. Misawa and S. Juodkazis, eds., *3D Laser Microfabrication: Principles and Applications* (John Wiley & Sons, 2006).
3. K. M. Davis, K. Miura, N. Sugimoto, and K. Hirao "Writing waveguides in glass with a femtosecond laser," Appl. Phys. Lett. **21**, 1729–1731 (1996).
4. K. Miura, J. R. Qiu, H. Inouye, T. Mitsuyu, and K. Hirao, "Photowritten optical waveguides in various glasses with ultrashort pulse laser," Appl. Phys. Lett. **71**, 3329–3331 (1997).
5. A. M. Streltsov, "Femtosecond-laser writing of tracks with depressed refractive index in crystals," in *Conference on Laser Micromachining for Optoelectronic Device Fabrication*, A. Ostendorf, ed., Proc. SPIE **4941**, 51–57 (2003).
6. I. Bennion, M. Dubov, I. Khruschev, A. Okhrimchuck, A. Shestakov, "Laser inscription of optical structures in crystals," Patent WO 2005040874 A2 (2005).
7. A. G. Okhrimchuk, A. V. Shestakov, I. Khrushchev, and J. Mitchell, "Depressed cladding, buried waveguide laser formed in a YAG:Nd3+ crystal by femtosecond laser writing," Opt. Lett. **30**, 2248–2250 (2005).
8. N. Dong, F. Chen, and J. R. Vàsquez de Aldana, "Efficient second harmonic generation by birefringent phase matching in femtosecond-laser-inscribed KTP cladding waveguides," Phys. Status Solidi (RRL) **6**, 306–308 (2012).
9. J. Hu and C. R. Menyuk, "Understanding leaky modes: slab waveguide revisited," Adv. Opt. Photon. **1**, 58–106 (2009).
10. H. Karakuzu, M. Dubov, and S. Boscolo, "Control of the properties of micro-structured waveguides in lithium niobate crystal," Opt. Express **21**, 17122–17130 (2013).
11. H. Karakuzu, M. Dubov, S. Boscolo, L. A. Melnikov, and Y. A. Mazhirina, "Optimisation of microstructured waveguides in z-cut $LiNbO_3$ crystals," Opt. Mater. Express **4**, 541–552 (2014).
12. S. M. Eaton, H. Zhang, M. L. Ng, J. Li, W.-J. Chen, S. Ho, and P. R. Herman, "Transition from thermal diffusion to heat accumulation in high repetition rate femtosecond laser writing of buried optical waveguides," Opt. Express **16**, 9443–9458 (2008).

#210200 - $15.00 USD Received 24 Apr 2014; revised 18 Jul 2014; accepted 19 Jul 2014; published 24 Jul 2014

13. S. M. Eaton, M. L. Ng, J. Bonse, A. Mermillod-Blondin, H. Zhang, A. Rosenfeld, and P. R. Herman, "Low-loss waveguides fabricated in BK7 glass by high repetition rate femtosecond fiber laser," Appl. Opt. **47**, 2098–2102 (2008).
14. M. Dubov "Direct femtosecond laser inscription in transparent dielectrics," PhD thesis, Aston University (2011).
15. T. Allsop, M. Dubov, V. Mezentsev, and I. Bennion, "Inscription and characterization of waveguides written into borosilicate glass by a high-repetition-rate femtosecond laser at 800 nm," Appl. Opt. **49**, 1938–1950 (2010).
16. S. Gross, M. Ams, D. G. Lancaster, T. M. Monro, A. Fuerbach, and M. J. Withford, "Femtosecond direct-write überstructure waveguide Bragg gratings in ZBLAN," Opt. Lett. **37**, 3999–4001 (2012).
17. S. Gross, M. Alberich, A. Arriola, M. J. Withford, and A. Fuerbach, "Fabrication of fully integrated antiresonant reflecting optical waveguides using the femtosecond laser direct-write technique," Opt. Lett. **38**, 1872–1874 (2013).
18. F. Chen and J. R. Vàsquez de Aldana, "Optical waveguides in crystalline dielectric materials produced by femtosecond-laser micromachining," Laser Photon. Reviews **8**, 251–275 (2014).
19. A. H. Nejadmalayeri and P. R. Herman, "Ultrafast laser waveguide writing: Lithium niobate and the role of circular polarization and picosecond pulse width," Opt. Lett. **31**, 2987–2989 (2006).
20. A. Fernandez, T. Fuji, A. Poppe, A. Furbach, F. Krausz, and A. Apolonski, "Chirped-pulse oscillators: a route to high-power femtosecond pulses without external amplification," Opt. Lett. **29**, 1366–1368 (2004).
21. R. Graf, A. Fernandez, M. Dubov, H. Brueckner, B. Chichkov, and A. Apolonski, "Pearl-chain waveguides written at megahertz repetition rate," Applied Physics B: Lasers and Optics **87**, 21–27 (2007).
22. A. G. Okhrimchuk, V. K. Mezentsev, H. Schmitz, M. Dubov, and I. Bennion, "Cascaded nonlinear absorption of femtosecond laser pulses in dielectrics," Laser Phys. **19**, 1415–1422 (2009).
23. V. Mezentsev, J. Petrovic, M. Dubov, I. Bennion, J. Dreher, H. Schmitz, and R. Grauer, "Femtosecond laser microfabrication of subwavelength structures in photonics," Proc. SPIE **6459**, 64590B (2007).
24. V. Mezentsev, M. Dubov, J. S. Petrovic, I. Bennion, J. Dreher, and R. Grauer, "Role of plasma in femtosecond laser pulse propagation," in *Physics of Ionized Gases* **876**, 169–180 (2006).
25. A. Turchin, M. Dubov, and J. A. R. Williams, "3d reconstruction of the complex dielectric function of glass during femtosecond laser micro-fabrication," Opt. Quantum Electron. **42**, 873–886 (2011).
26. B. P. Cumming, A. Jesacher, M. J. Booth, T. Wilson, and M. Gu, "Adaptive aberration compensation for three-dimensional micro-fabrication of photonic crystals in lithium niobate," Opt. Express **19**, 9419–9425 (2011).
27. M. J. Booth, M. Schwertner, T. Wilson, M. Nakano, Y. Kawata, M. Nakabayashi, and S. Miyata, "Predictive aberration correction for multilayer optical data storage," Appl. Phys. Lett. **88**, 031109 (2006).
28. M. Dubov, I. Bennion, D. Nikogosyan, P. Bolger, and A. Zayats, "Point-by-point inscription of 250 nm period structure in bulk fused silica by tightly focused femtosecond uv pulses," J. Opt. A: Pure Appl. Opt. **10**, 025305 (2008).
29. M. Dubov, V. Mezentsev, I. Bennion, and D. N. Nikogosyan, "UV femtosecond laser inscribes a 300 nm period nanostructure in a pure fused silica," Meas. Sci. Technol. **18**, L15 (2007).
30. K. Nugent, "Wave field determination using 3-dimensional intensity information," Phys. Rev. Lett. **68**, 2261–2264 (1992).
31. A. Barty, K. A. Nugent, D. Paganin, and A. Roberts, "Quantitative optical phase microscopy," Opt. Lett. **23**, 817–819 (1998).
32. A. Roberts, E. Ampem-Lassen, A. Barty, K. Nugent, G. Baxter, N. Dragomir, and S. Huntington, "Refractive-index profiling of optical fibers with axial symmetry by use of quantitative phase microscopy," Opt. Lett. **27**, 2061–2063 (2002).
33. E. Ampem-Lassen, S. Huntington, N. Dragomir, K. Nugent, and A. Roberts, "Refractive index profiling of axially symmetric optical fibers: a new technique," Opt. Express **13**, 3277–3282 (2005).
34. J. S. Petrovic, V. Mezentsev, H. Schmitz, and I. Bennion, "Model of the femtosecond laser inscription by a single pulse," Opt. Quantum Electron. **39**, 939–946 (2007).
35. W. Yang, P.G. Kazansky, and Yu.P. Svirko, "Non-reciprocal ultrafast laser writing," Nat. Photon. **2**, 99–104 (2008).

1. Introduction

Owing to its robustness and unique flexibility, the direct femtosecond (fs) laser inscription method [1, 2] is one of the most efficient techniques for three-dimensional volume microstructuring of transparent dielectrics, thereby offering a valuable alternative to more mature technology such as, for instance, lithography-based approaches. A pioneering demonstration of the possibility of modifying the refractive index (RI) of glasses in a controlled manner by use of intense fs laser pulses was reported in [3, 4]. Photoinduced structural modification of glasses has triggered the research in this field, and is the foundation for all subsequent applications of such a technology in integrated optics. In crystals the exposure to fs laser radiation often pro-

#210200 - $15.00 USD Received 24 Apr 2014; revised 18 Jul 2014; accepted 19 Jul 2014; published 24 Jul 2014

duces a negative change in the RI [5, 6] which does not allow for waveguiding to be observed directly in single written tracks. On the other hand, by writing multiple tracks with a reduced RI around the unmodified volume of material it is possible to produce a depressed-index cladding with the central volume serving as the core of a waveguide (WG) [6, 7]. The depressed cladding fs-laser inscription approach can in principle achieve arbitrarily shaped light guiding channels inside the unmodified material [6], which feature reduced propagation losses (due, e.g., to induced material absorption or scattering [1, 8]) as compared to directly written, single-track WGs [7]. The main issue with this approach is how to ensure good mode confinement in the WG, as depressed-index cladding WGs often exhibit leaky-mode features [9], especially when the thickness of the cladding structure or the magnitude of RI contrast between the low-index tracks of the cladding structure and the core guiding region is small. We have addressed this issue in recent numerical works [10, 11]. We have demonstrated to which extent the waveguiding properties of depressed cladding WGs written in birefringent crystals can be controlled by the WG geometry at the induced RI contrasts that are feasible by use of current fs microfabrication technology [10], and described how these properties can be optimized for low-loss operation in the mid-infrared spectrum [11].

In this paper, we report on the operational parameters that are required to fabricate such a low-loss, buried, microstructured WG in a crystal of great importance for applications in nonlinear integrated optics, lithium niobate ($LiNbO_3$), by high-repetition-rate (HRR) fs laser inscription. The observations and results described here serve to support our numerical studies in [10, 11]. HRR fs lasers have become the preferred laser source for fast writing of low-loss WGs in glasses [12–17], enabling RI contrasts between exposed and unexposed areas of up to five times higher than those of standard optical fibers [14, 15]. However the application of this approach to crystals has received less attention in the literature [18]. We would also like to note that the energy efficiency of HRR laser systems can be twice as large as that of low-repetition-rate (LRR) systems owing to the heat accumulation effect [12, 13]. At HRRs, the time between successive laser pulses is shorter than the heat dissipation or cooling time, resulting in an accumulation of heat in the focal volume that melts the material. This melted zone is sustained above the working point of the material throughout the laser cycle, which can be beneficial for smooth track formation. As the laser is scanned through the sample, the molten material cools from the outside in, resulting in a permanent RI change. The key control parameter for permanent material modification seems to be the energy density delivered into the focal volume which drives all subsequent material transformations [14, 19]. kHz fs laser systems which are currently most widely used for WG writing in crystals, employ typical sample translation speeds of 10 to a few hundred μm/s. The slow laser writing at LRRs is the main limiting factor for the experimental exploration of complex depressed cladding WG designs suitable for practical applications. Indeed, typical structures that have been fabricated to date mostly consist of either just two parallel tracks or a single layer of circularly arranged tracks confining an unmodified domain of crystal, and usually suffer from high propagation losses [8, 18]. Furthermore, such structures do not allow for flexible control over the waveguiding properties. On the other hand, HRR fs systems can enable up to four orders of magnitude quicker fabrication than the LRR ones [14, 15]. This makes feasible the fabrication of more complex depressed cladding WG structures having a fairly large number of layers of tracks and thereby displaying low-loss operation over a wide spectral range [10].

2. Experimental setup and procedures

The experimental setup used for inscription is shown in Fig. 1. The inscribing laser was a chirped-pulse oscillator system [20] (Femtosource Scientific XL, Femtolasers), which operates at 792 nm central wavelength and is pumped with a diode-pumped solid state Verdi V-10

#210200 - $15.00 USD Received 24 Apr 2014; revised 18 Jul 2014; accepted 19 Jul 2014; published 24 Jul 2014

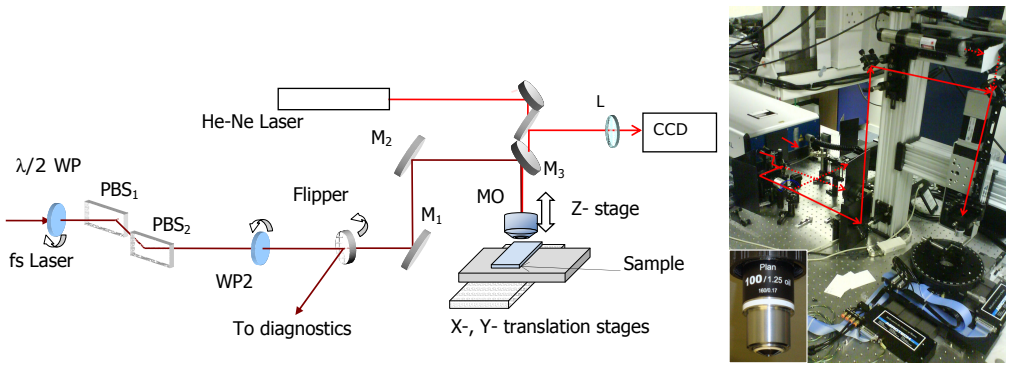

Fig. 1. Optical schematic and photograph of the experimental setup. The insert on the photo presents the oil-immersed MO used for inscription in lithium niobate crystals. WP stands for: wave plate, PBS: polarization-beam splitter, M: folding mirror, MO: micro-objective, CCD: charge-couple device camera.

(10 W) green, 532 nm laser. The repetition rate of the fs laser is 11 MHz. The temporal pulse widths of individual pulses were measured using a frequency-resolved optical gating technique (Grenouille). The use of broadband, highly chirped mirrors in the laser cavity enables the compensation of the dispersion of all intra-cavity components and the achievement of a full-width at half-maximum pulse duration of approximately 50 fs, that being the shortest pulse width obtainable with a reasonably radially symmetric beam profile and a saturable Bragg reflector (SBR) end mirror [15]. For this pulse width, the spectral bandwidth is approximately 30 nm (at 10% intensity level). Wider spectra (hence shorter pulses) seem to constitute a problem for this system due to the limitations imposed by the SBR. Overall, the optical microfabrication system used enables on-target pulse energies of up to 75 nJ. Without the SBR, the same system produces 26 fs pulses with more than twice the output energy [20, 21]. Several microscope objective lenses were used to produce index modifications in the $LiNbO_3$ crystal. After some preliminary trials aimed at producing smooth, non-damaged tracks, it was decided to use an objective with a numerical aperture (NA) of 1.25 and a working distance of approximately 0.4 mm (Fig. 1). This is a Zeiss oil-immersed objective (RI of oil used: $n = 1.523$) with a fixed correction of spherical aberration at the depth of 0.17 mm in standard glass. Additional dispersion induced by the glass of the objective was pre-compensated by tuning the prism compressor at the laser output. We would like to note that in contrast to previous reports on laser WG writing in $LiNbO_3$ [19], we used linear polarization of the inscribing light perpendicular to the sample scanning direction, and almost transform-limited fs pulses. Our choice was based on several experiments in various glasses [14, 15] and crystals [14, 22], which revealed that the optimum regimes of HRR fs inscription are essentially independent of the inscribing polarization state. *z*-cut $LiNbO_3$ wafers of 75 mm diameter and 1 mm thick (supplied by University Wafer) were used in the experiments. The samples were mounted on a three-dimensional Aerotech translation stage, comprising two air-bearing stages for the *x* and *y* directions and a mechanical stage for the *z* direction, and enabling translation speeds of up to 100 mm/s with a sub-micrometer accuracy. The samples were moved transversely to the laser beam (in the *x*, *y* plane), and accurate positioning of the sample relative to the objective along the direction of the fs beam was controlled using the reflection from the sample top surface. Only the working distance of the objective lens limited the maximum depth of inscription from the sample's surface to approxi-

#210200 - $15.00 USD Received 24 Apr 2014; revised 18 Jul 2014; accepted 19 Jul 2014; published 24 Jul 2014

mately 0.5 mm. A more detailed description of the experimental setup used for inscription can be found in [14].

Note that the better the focusing of the fs beam onto the sample to be inscribed, the lower the pulse energy above which a continuum light is produced within the material for a given inscription depth [23, 24]. In borosilicate (BK7) glass, using an in-house designed, long working distance, oil-immersed microscope objective with an effective NA of 1.2 [25], we measured this energy threshold to be approximately 12 nJ at an inscription depth of 0.5 mm, whereas in $LiNbO_3$ (and with the 1.25 NA of the commercial objective) the threshold was three times higher at an inscription depth of approximately 0.25 mm. In $LiNbO_3$, as well as in other crystals [22], the energy threshold for the appearance of a continuum is slightly lower than the threshold for residual material modification to occur. The conditions of fs beam focusing are critical for direct inscription in $LiNbO_3$ crystals [26], as the RI of the extraordinary axis (z axis) differs significantly from that of the ordinary axes. Diffraction-limited focusing in birefringent crystals is itself a challenging task, because an aberration-free focusing at an arbitrary depth in such crystals is not possible by standard microscope objectives. Adaptive optics (such as, e.g., deformable mirrors) [27] or computer-controlled spatial phase modulators [26] may be used for correction of the aberration, and a feedback loop for the corrective system is needed. However, most of the quantitative feedback methods that are available to determine the optimum focusing conditions are not applicable to birefringent hosts. In the inscription experiments described in this paper, we used a qualitative feedback method based on either measurement by a photodiode or naked eye visual perception (using appropriate filter or protective glasses) of the brightness of continuum light produced within the sample. The decision about the microscope objective was made based upon the lowest energy threshold provided for the appearance of a continuum.

The irradiated samples were visually inspected with an optical microscope, Axioscope-2 MOT (Zeiss), which is equipped for both transmitted light and differential interference contrast (DIC) measurements. The 16-bit, 10 M-pixel charge-couple device (CCD) camera of the microscope is interfaced to a personal computer by a fibre-optic link, which reduces the level of electronic noise and achieves high data throughput. The capabilities of the microscope are described in detail in [28, 29]. The sample tracks were inspected using the quantitative phase microscopy (QPM) method [30, 31] at the microscope (commercial software by IATIA), from which a cumulative phase profile and, hence, refractive index distribution over the radial distance from the central axis of the track can be obtained. The QPM technique relies on taking multiple images of the intensity distribution of the field leaving a phase object at different focus distances (an in-focus image and a number of slightly positively and negatively defocused images) and using these data to estimate the differential with respect to the defocus of the image for phase recovery [30, 32]. Thus, it is clear that accurate positioning of the object along the z axis is very important for the extraction of correct phase information. In its motorized version, the microscope has a built-in, electronically controlled z translation stage with an approximate positioning accuracy of 100 nm. To achieve even better z stage performance, we used a z step size equaling an integer multiple of the step size of the stepper motor, thus avoiding any interpolation by the motion controller. This way we were able to improve the positioning accuracy up to the (estimated) value of 20 nm. This could be further improved by a position feedback encoder. Obviously, any noise arising during image acquisition and transmission should also be reduced to minimum. Because the CCD camera of the microscope is uncooled, for short exposure times a few low-order bits are indistinguishable. We found that this noise can be minimized by choosing exposure times of a large fraction of a second. The QPM procedure was calibrated by measuring optical fibres with known specifications at different illumination wavelengths to ensure minimum chromatic aberrations of the system. Multi-layer Fabri-Perot interference filters (Semrock) with an approximate bandwidth of 20 nm were used to limit the bandwidth of

#210200 - $15.00 USD Received 24 Apr 2014; revised 18 Jul 2014; accepted 19 Jul 2014; published 24 Jul 2014

the light source of the microscope. The sensitivity of the QPM method was tested on WGs fabricated in BK7 glasses by direct fs inscription. We believe that the current sensitivity level is of the order of 10^{-5} [25], which is *below* that of a conventional DIC microscope [29]. However, care should be taken when the QPM technique is applied to objects with absorption (represented by the imaginary part of the permittivity). This is because the QPM method is based on the transport-of-intensity equation [30, 31], which is valid only when the beam energy is preserved. A comparison of QPM measurements of BK7 glasses with those obtained by scattering interferometry clearly highlights this problem [25].

The radial refractive index profiles of the tracks were reconstructed from the cumulative phase data obtained from QPM using the Abel inverse transform method [33]. To implement an Abel transform, it must be assumed that the structure is radially symmetric about its axis. A visual inspection of the cross section of the tracks suggested this to be a reasonable assumption. This assumption in the case of BK7 glass was further confirmed by comparison of mode-field profile measurements with the results of numerical simulations for a number of tracks. The reconstructed RI values were used in the numerical model in each case. By the use of QPM and the inverse Abel transform it is possible to obtain phase retardation maps over the whole field of view of the microscope, which has the approximate size $300\,\mu\text{m} \times 400\,\mu\text{m}$ for an image magnification factor of 20, at the same time as qualitatively inspecting the results of the inscription under the microscope, thereby making the time required for post-inscription processing of the samples shorter [15]. We would like to note that the phase retardation maps obtained from the QPM software for *z*-cut $LiNbO_3$ samples are not sensitive to the polarization of the illumination light. For wafers of different orientation, care should be taken when interpreting the phase maps because of the host birefringence.

3. Results and discussion

The parameter space that was investigated to establish the optimal conditions for inscription included the inscribing laser pulse energy, the speed of translation stage movement, the focus depth inside the sample, the polarization of the inscribing light relative to the direction of the scanning laser beam, and the duration of the inscribing pulses. For the results described in this paper, the inscribing beam was polarized in the x direction perpendicular to the direction of scanning, and provided pulses with the minimal (transform-limited) pulse duration (Sec. 2). The inscribing beam profile featured a small ellipticity (defined as $1 - b/a$, where a and b are the respective major and minor semi-axes) of 0.05, with the larger semi-axis in the scan (y) direction [22].

Figure 2(a) shows example tracks obtained with a high inscription energy. The tracks of each of the two pairs shown were written with the same scanning speed, but with opposite scan directions. No significant morphological changes of the tracks are observed depending on the scan direction in the *z*-cut $LiNbO_3$ crystal, and highly uniform tracks are obtained even at high sample inscription speeds. A typical example of the reconstructed radial index profile of tracks written with high energies is shown in Fig. 2(b). To identify the inscription conditions (both inscription energies and scanning velocities at specific depths from the crystal's surface) for high-contrast, uniform tracks, the uniformity of each track was inspected using the phase maps obtained from QPM. The QPM software allows one to generate artificial DIC images of the tracks with an arbitrary direction of differentiation. By this approach, we were able to determine the onset of instability when a track starts to become (aperiodically) modulated. This instability is likely due to an elongation of the 'melted tail' of the track being exposed to a high mechanical stress from the cold surrounding material, which occurs for increased inscription energies and scanning speeds. It was numerically found in [34] that the magnitude of this stress can reach hundreds of megapascals. Such compressive forces act as an effective surface tension

#210200 - $15.00 USD Received 24 Apr 2014; revised 18 Jul 2014; accepted 19 Jul 2014; published 24 Jul 2014

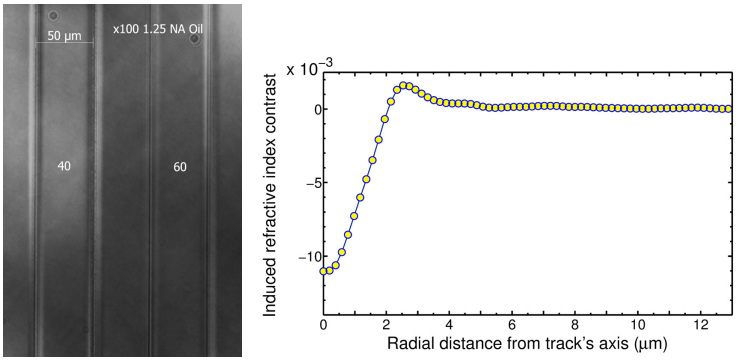

(a) (b)

Fig. 2. (a) DIC microscope overhead views of two pairs of tracks with the same inscription energy of 58 nJ and with scanning speeds of 40 mm/s (left pair) and 60 mm/s (right pair) inscribed at an approximate depth of 200 μm. The tracks of each pair were inscribed with opposite scan directions. (b) Radial RI profile of a track reconstructed from the cumulative phase data obtained from QPM. Writing conditions for this track were inscription energy 58 nJ, scan velocity 12 mm/s and inscription depth $\approx 200\,\mu$m.

leading to various thermoelastic and, possibly, hydrodynamic instabilities of the softened or even melted jet.

The physical characteristics of all the tracks obtained with different inscription conditions except those showing apparent instabilities, were measured by white-light microscope and the QPM technique using the Abel transform. Figure 3 shows the radial size (r) and the peak index contrast (δn; measured from the zero level) as a function of inscription energy (E) for tracks produced with a scanning inscription velocity of 12 mm/s at an approximate depth of 250 μm from the surface of the crystal. It is seen that both the track's size and the magnitude of the peak index clearly increase with pulse energy. The maximum index change observed is -0.0127 for an inscription energy of 58 nJ. This is the first time to our knowledge that such a high RI contrast has been achieved for smooth tracks in $LiNbO_3$. A linear fit to the experimental data in Fig. 3 yields the following functions:

$$r = 9.65\times10^{-2}\,(E-E_{\rm th})\,, \quad \delta n = -4.46\times10^{-4}\,(E-E_{\rm th})\,, \tag{1}$$

where r is given in micrometers, E is given in nanojules, and $E_{\rm th} = 36.45$ nJ is the energy threshold of the microscope objective used for inscription. These fitting functions were used for numerical optimization of microstructured WGs in [11]. Note that the interdependence of the track's size and RI contrast at a given scanning speed stemming from Fig. 3 can be released, and these parameters can be trimmed to the desired values by tuning both the laser pulse energy and the sample inscription speed, as both produce albeit connected but not identical changes to r and δn. We got evidence that uniform tracks can be achieved within a wide range of scanning velocities – from a few mm/s to 60 mm/s. However, at high speeds, the uniformity of the immersion layer underneath the microscope objective becomes an issue, with this effect being more pronounced at high pulse energies. Therefore, we believe that the practically interesting inscription regimes in $LiNbO_3$ are close to those illustrated by Fig. 3.

In order to create microstructured WGs with the desired geometry, one needs to control the relative positions of the tracks at the desired inscription depth beneath the sample surface with high precision. There is not a simple linear relationship between the actual depth of focusing of the inscribing light and the shift of the microscope objective produced by the z-axis stage.

#210200 - $15.00 USD Received 24 Apr 2014; revised 18 Jul 2014; accepted 19 Jul 2014; published 24 Jul 2014

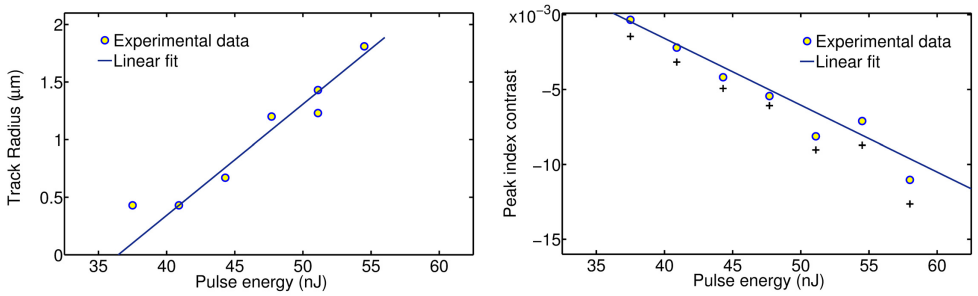

(a) (b)

Fig. 3. (a) Radius and (b) reconstructed peak RI contrast of the tracks as a function of inscription energy at an inscription scanning velocity of 12 mm/s and an approximate inscription depth of 250 μm. Also shown is the energy dependence of the peak-to-peak index contrast (crosses).

However, effective control over the track's positioning for producing circular patterns of tracks can be achieved by measuring the eccentricity ε of the resultant WG's cross section after edge polishing of the sample. After that, the z coordinate of each track in the original (circularly shaped) design is scaled by ε, and this scaling factor is used by the program that controls the z-coordinates of the tracks relative to the center of the structure. For inscription of circular patterns of tracks at an approximate depth of 400 μm, we measured $\varepsilon \approx 0.7$, with the larger axis of the elliptical pattern in the x direction (Fig. 4(b)). Figure 4 shows the microscope images of an example microstructured WG written with an energy of 48 nJ, scanning velocity of 15 mm/s, and at an approximate depth of 400 μm. The depressed cladding is formed by two rings of sixteen tracks each, whose centers are arranged circularly. The designed radii of the inner and outer circles are 24 μm and 30 μm. The measured major and minor axis of an an individual track are approximately 3.7 μm and 1.4 μm, respectively. Further, we would like to note that some focus splitting effects were observed in our experiments (Fig. 4 (b)), typically at elevated laser pulse energies and for certain z-positions, e.g. when we focused deeper than 300 μm. Such a splitting as well as observed elongation of the individual track are most likely due to changes in the trade-off among aberrations, nonlinearity and, possibly, other effects [35] in the $LiNbO_3$ crystal host at different inscription depths.

The waveguiding properties were investigated by illuminating the structure with a broadband supercontinuum (SC) source with a total bandwidth from 400 to 2000 nm (supplied by Fianium). Light from the source was filtered by an external acousto-optic tunable filter having up to eight independent wavelength channels, each of approximate width 20 nm. The filtered SC light was coupled into a multi-mode optical fiber with a core diameter of 40 μm. The estimated total propagation losses were approximately 3 dB/cm at visible wavelengths around 600 nm, whereas they were approximately ten times larger (on a linear scale) at wavelengths around 1000 nm. The estimation of the losses was made by integrating the mode-field profile on the CCD camera. The observed behavior has been confirmed by our numerical study [10]. The weaker guiding at the longer wavelength was expected as the proof-of-principle WG structure of Fig. 4 with only two rings of tracks was designed intuitively rather than using a systematic approach [11].

Because the RI contrasts of smooth tracks that can be achieved in crystals with current fs microfabrication technology are relatively moderate, to provide WG structures that display low-loss operation over a wide spectral range, the most viable solution is to write a fairly large number of rings of tracks, possibly with different sizes [10]. Optimized designs of WG struc-

#210200 - $15.00 USD Received 24 Apr 2014; revised 18 Jul 2014; accepted 19 Jul 2014; published 24 Jul 2014

tures with several cladding layers were numerically shown to achieve acceptably low (below 1 dB/cm) confinement losses (i.e., losses due to the finite transverse extent of the confining structure) in both O and E polarizations over a wide spectral range, extending into the mid-infrared region up to the end of the transparency range of the host material [11]. We are currently working on the experimental demonstration and characterization of such optimized WG designs. The results will be presented in a future publication. We would like to note that the requirements on the number of rings make HRR fs laser inscription the preferred microfabrication technique. For example, for a propagation length of 10 cm in a WG with seven rings (around 200 tracks) the total length of the inscribed lines would amount to approximately 20 m. Clearly, if one uses a kHz fs system (with a typical sample translation speed of 10 to 100 μm/s, or of 500 μm/s by use of astigmatic beam inscription [22]), the fabrication time required on a single structure may exceed 60 hours, whereas a HRR system can do the job in less than an hour. It is also clear that the HRR fs laser microfabrication technology described in this paper can be easily extended to periodically poled crystals, thereby enabling a wide spectrum of applications in classical and quantum nonlinear integrated optics.

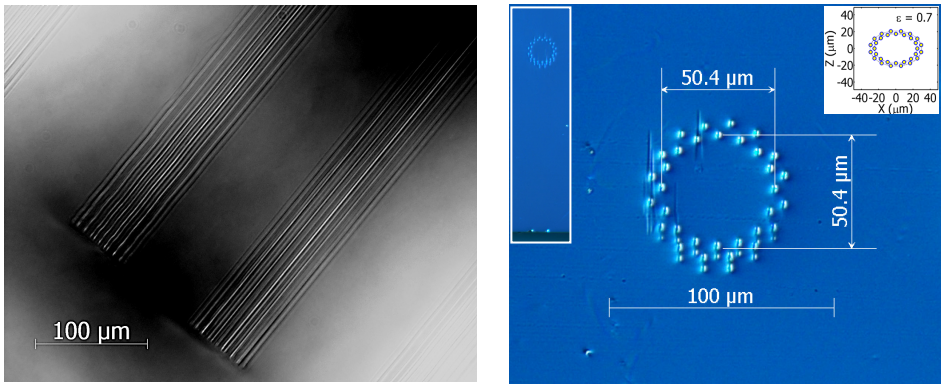

a) b)

Fig. 4. Microscope (a) overhead view, and (b) cross section of an example fabricated microstructured WG with two rings of tracks. Fabrication conditions for this WG were inscription energy 48 nJ, scan velocity 15 mm/s, and inscription depth $\approx 400\,\mu$m. The left inset in panel (b) highlights the inscription depth, and the right inset in (b) shows the WG design scaled by the ellipticity factor ε.

4. Conclusions

We have reported on the inscription regimes that are required to fabricate low-loss, buried, microstructured WGs in z-cut $LiNbO_3$ crystals by an HRR fs laser system. Record-high RI contrasts of -0.0127 have been obtained for individual modification tracks. These results offer promising means for the development of microstructured WGs in nonlinear crystals which are suitable for integrated optics applications in both the near- (telecommunications) and mid-infrared spectral regions. Demonstration of such optimized WG designs in both unpoled and poled hosts will be presented in a future work.

Acknowledgments

We acknowledge support by the Leverhulme Trust (grant RPG-278) and the Engineering and Physical Sciences Research Council (EPSRC grant EP/J010413/1).